Computational and Structural Biotechnology Journal 27 (2025) 887–895

Contents lists available at ScienceDirect

Computational and Structural Biotechnology Journal

journal homepage: www.elsevier.com/locate/csbj

Research Article

Repurposing thioridazine as a potential CD2068 inhibitor to mitigate antibiotic resistance in *Clostridioides difficile* infection

Methinee Pipatthana [a], Matthew Phanchana [b], Apiwat Sangphukieo [c], Sitthivut Charoensutthivarakul [d,e,f], Phurt Harnvoravongchai [g], Surang Chankhamhaengdecha [g], Pattaneeya Prangthip [h], Pattanai Konpetch [i], Chanakarn Sripong [j], Sarawut Wongphayak [k], Tavan Janvilisri [i,*]

[a] *Department of Microbiology, Faculty of Public Health, Mahidol University, Bangkok, Thailand*
[b] *Department of Molecular Tropical Medicine and Genetics, Faculty of Tropical Medicine, Mahidol University, Bangkok, Thailand*
[c] *Center of Multidisciplinary Technology for Advanced Medicine, Faculty of Medicine, Chiang Mai University, Chiang Mai, Thailand*
[d] *Excellence Center for Drug Discovery (ECDD), Faculty of Science, Mahidol University, Bangkok, Thailand*
[e] *School of Bioinnovation and Bio-Based Product Intelligence, Faculty of Science, Mahidol University, Bangkok, Thailand*
[f] *Center for Neuroscience, Faculty of Science, Mahidol University, Bangkok, Thailand*
[g] *Department of Biology, Faculty of Science, Mahidol University, Bangkok, Thailand*
[h] *Department of Tropical Nutrition and Food Science, Faculty of Tropical Medicine, Mahidol University, Bangkok, Thailand*
[i] *Department of Biochemistry, Faculty of Science, Mahidol University, Bangkok, Thailand*
[j] *Samitivej Srinakarin Hospital, Bangkok, Thailand*
[k] *Vishuo Biomedical (Thailand) Ltd., Bangkok, Thailand*

ARTICLE INFO

Keywords:
Nucleotide-binding domain inhibitor
Drug repurposing
Virtual screening
Antibiotic resistance

ABSTRACT

Clostridioides difficile infection (CDI) is a major public health issue, driven by antibiotic resistance and frequent recurrence. CD2068, an ABC protein in *C. difficile*, is associated with drug resistance, making it a potential target for novel therapies. This study explored FDA-approved non-antibiotic drugs for their ability to inhibit CD2068 through drug screening and experimental validation. Thioridazine exhibited moderate binding affinity to CD2068 and inhibited its ATP hydrolysis activity. It also suppressed the growth of multiple *C. difficile* ribotypes at 64–128 μg/mL, with rapid-killing effects. When combined with sub-MIC levels of standard antibiotics, thioridazine significantly reduced bacterial growth. In a mouse CDI model, thioridazine demonstrated potential in restoring gut microbial balance and improving survival, although it did not show superiority to vancomycin. These findings suggest that thioridazine has potential as a novel therapeutic for CDI, either as an adjunct to existing antibiotics or as part of a combination therapy to combat antibiotic resistance. Further research, including replication studies and dose optimization, is needed to fully evaluate thioridazine's therapeutic potential.

1. Introduction

Clostridioides difficile causes antibiotic-associated diarrhea, with infections spiking due to broad-spectrum antibiotics disrupting gut eubiosis [1]. CDI severity ranges from mild to life-threatening, causing severe diarrhea, colitis, toxic megacolon, sepsis, and death. Antibiotic resistance has made treatment challenging, necessitating new, effective treatments and preventive measures. *C. difficile* shows high resistance not only to the recommended CDI drugs, but also to common antibiotics like clindamycin, erythromycin, tetracycline, fluoroquinolones, and rifamycins [2]. *C. difficile* employs various resistance mechanisms, including drug inactivation, target modification, and efflux pumps [3]. A notable mechanism involves ATP-binding cassette (ABC) transporters, which use ATP to transport compounds, promoting bacterial survival under toxic conditions. In *C. difficile*, 230 putative ABC proteins have been identified, forming at least 78 complete systems [4]. Half of these ABC systems are predicted to be involved in the extrusion of antimicrobial compounds. However, only CD2068 has been experimentally

* Corresponding author.
E-mail address: tavan.jan@mahidol.ac.th (T. Janvilisri).

https://doi.org/10.1016/j.csbj.2025.02.036
Received 8 November 2024; Received in revised form 26 February 2025; Accepted 27 February 2025
Available online 1 March 2025

validated for its role in antimicrobial resistance and substrate specificity. It has been shown that CD2068 mediates multidrug efflux in *C. difficile* [5]. *CD2068* knockout in *C. difficile* significantly increases sensitivity to various antibiotics. Moreover, CD2068 overexpression in *Escherichia coli* promotes drug efflux, indicating its role in drug resistance in *C. difficile*. Thus, CD2068 is a potential target candidate for drug development for reversal of antibiotic resistance in *C. difficile*.

To date, only three drugs including fidaxomicin, vancomycin, and metronidazole are approved for treatment of CDI by the US Food and Drug Administration (FDA). Prolonged use of these drugs together with the development of resistance mechanisms by this bacterium render inefficient treatment, resulting in the update guidelines on management of *C. difficile* infection [6]. Therefore, a new therapeutic option is certainly needed to cope with this circumstance. One effective strategy to overcome antibiotic resistance caused by ABC proteins is through the discovery of inhibitors to impede the functioning of the ABC proteins. Basically, the development of novel and potent drugs is an expensive, complicated, and time-consuming process. High throughput *in silico* virtual screening of FDA approved drug libraries has become a powerful tool to identify potential drug candidates prior to further validations. As the approved drugs are proven as safe for clinical use, it drastically shortens the drug discovery pipeline.

Here, we aimed to identify a candidate targeting the multidrug resistance ATPase protein, CD2068, through *in silico* virtual screening of a FDA-approved drug library. The model structure of CD2068 was first constructed, and a hit compound was characterized *in vitro* and *in vivo*. The lead compound identified may potentially serve as an inhibitor to reverse antibiotic resistance of *C. difficile*.

2. Materials and methods

2.1. CD2068 modelling and virtual drug screening

Homology modeling and *de novo* prediction approaches from SWISS-MODEL [7], i-TASSER [8], trRosetta [9], Robetta [10], ModWeb [11], RoseTTAFold [12], and AlphaFold [13] were used. Predicted structures were compared with mTM-align [14] and visualized using UCSF ChimeraX [15]. For virtual screening, SeeSar and AutoDock Vina [16] were employed. We obtained 1094 small molecule structures (300–600 Da, approved in the US, Canada, and the EU) from the DrugBank database [17]. The CD2068 model and ligands were prepared using AutoDockTools and Open Babel [18], respectively. Virtual screening with AutoDock Vina focused on the ATP binding site of the i-TASSER-2 model. Hits were selected based on binding energy (AutoDock Vina) and a binding affinity cut-off below 500 nM (SeeSar). Molecular dynamic (MD) simulation of CD2068 with thioridazine was performed by Desmond MD (Schrödinger, LLC) [19]. The complex was prepared by protonation at pH 7, solvation with TIP3P water model and Na^+ and Cl^- to 150 mM, and protein neutralization with 22 Na^+. The system was relaxed by Desmond default parameter before MD simulation for 500 ns using MTK barostat for NPT ensemble at 300 K and 1 ATM.

2.2. Validation of drug binding to CD2068

CD2068 protein was purified from *E. coli* Rosetta (DE3) containing the pET28a-CD2068 plasmid. The culture was grown at 37°C until an OD_{600} of ~0.6, then induced with 1 mM IPTG and maintained at 20°C for 20 hours. After cell lysis, supernatant was loaded onto the Ni-NTA column, and CD2068 was eluted with buffer supplemented with imidazole, followed by dialysis to remove imidazole residues. Differential scanning fluorimetry (DSF) was used to screen hit compounds for interaction with CD2068. Conducted in assay buffer, the DSF involved 20 μM CD2068 protein, 5 × SYPRO Orange, and 500 μM hit compound in a 96-well PCR plate. Fluorescent signals were recorded across a temperature range of 25 – 95°C. The apparent melting temperature (T_{ma}) was calculated, and ΔT_{ma} values were determined as the difference between the T_{ma} of the DMSO control and the protein with the test compound. The threshold for ΔT_{ma} was set at 5 × the standard deviation of the T_{ma} of the DMSO control. Isothermal titration calorimetry (ITC) assessed the thermodynamics of protein-ligand interactions, with ligands titrated against 100 μM CD2068 using a Malvern MicroCal PEAQ-ITC at 25C. Data were analyzed using ITC analysis software.

2.3. ATPase activity

The ATPase activity of CD2068 was measured using a modified malachite green method [20]. Inorganic phosphate was quantified after adding 1 mM ATP to a reaction mixture with 1 μg of purified CD2068 in 50 mM HEPES (pH 7.4) and 5 mM $MgSO_4$. ATP hydrolysis occurred at 37°C for 5 minutes with varying thioridazine concentrations. The reaction was stopped with 0.76 mM malachite green in 0.35 % polyvinyl alcohol and 28 mM ammonium heptamolybdate diluted in 2.1 M H_2SO_4. After 20 minutes of dark incubation, inorganic phosphate levels were determined by absorbance at 595 nm, comparing thioridazine's inhibitory effect to a control.

2.4. Antibiotic susceptibility

C. difficile was cultured on cycloserine-cefoxitin fructose agar (CCFA) under anaerobic conditions (80 % N_2, 10 % CO_2, and 10 % H_2) at 37°C for 2 days. Colonies were then grown in brain heart infusion medium with 0.5 % yeast extract (BHIY). The minimum inhibitory concentration (MIC) of drugs against various *C. difficile* ribotypes was determined using the broth microdilution method [21]. Cultures were transferred to BHIY, grown to log-phase, and seeded into a 96-well plate with thioridazine. Plates were incubated anaerobically at 37°C for 48 hours. MIC was the lowest thioridazine concentration inhibiting growth compared to controls.

2.5. Time-kill analysis

C. difficile was cultured as described above and seeded to obtain ~6×10^6 CFU/mL in a 96-well plate containing the drug at MIC values: 64 μg/mL thioridazine, 4 μg/mL vancomycin, 0.5 μg/mL metronidazole, and 0.0625 μg/mL fidaxomicin. The remaining viable cells were kinetically measured by OD_{600} every 10 minutes for 6 hours under anaerobic conditions. Relative growth of *C. difficile* was calculated by dividing the OD_{600} at each time point (T_n) by the OD_{600} at the initial time point (T_0). The killing kinetics of thioridazine was compared to those of the control drugs.

2.6. Drug combination assay

The synergism or antagonism of thioridazine with vancomycin, metronidazole, or fidaxomicin was evaluated using a checkerboard assay. Thioridazine and each antibiotic were 2-fold serially diluted in BHIY and mixed. *C. difficile* culture was seeded into a 96-well plate with the drug combinations to obtain 1×10^5 CFU/well. Plates were incubated anaerobically for 48 hours, and turbidity was measured at OD_{600}. The fractional inhibitory concentration index (FICI) was calculated: $FICI = FIC_A + FIC_B$, where $FIC_A = C_A/MIC_A$ and $FIC_B = C_B/MIC_B$. MIC_A and MIC_B are the MICs of drugs A and B alone, respectively, while C_A and C_B are the concentrations of the drugs in combination. FICI values [22]: synergistic (≤ 0.5); additive (> 0.5 and < 1); indifferent (> 1 and ≤ 4); antagonistic (> 4). Thioridazine's effect with each antibiotic on *C. difficile* growth was monitored at OD_{600} every 10 minutes for 16 hours.

2.7. CDI experiment model

The CDI mouse model was conducted as detailed previously with

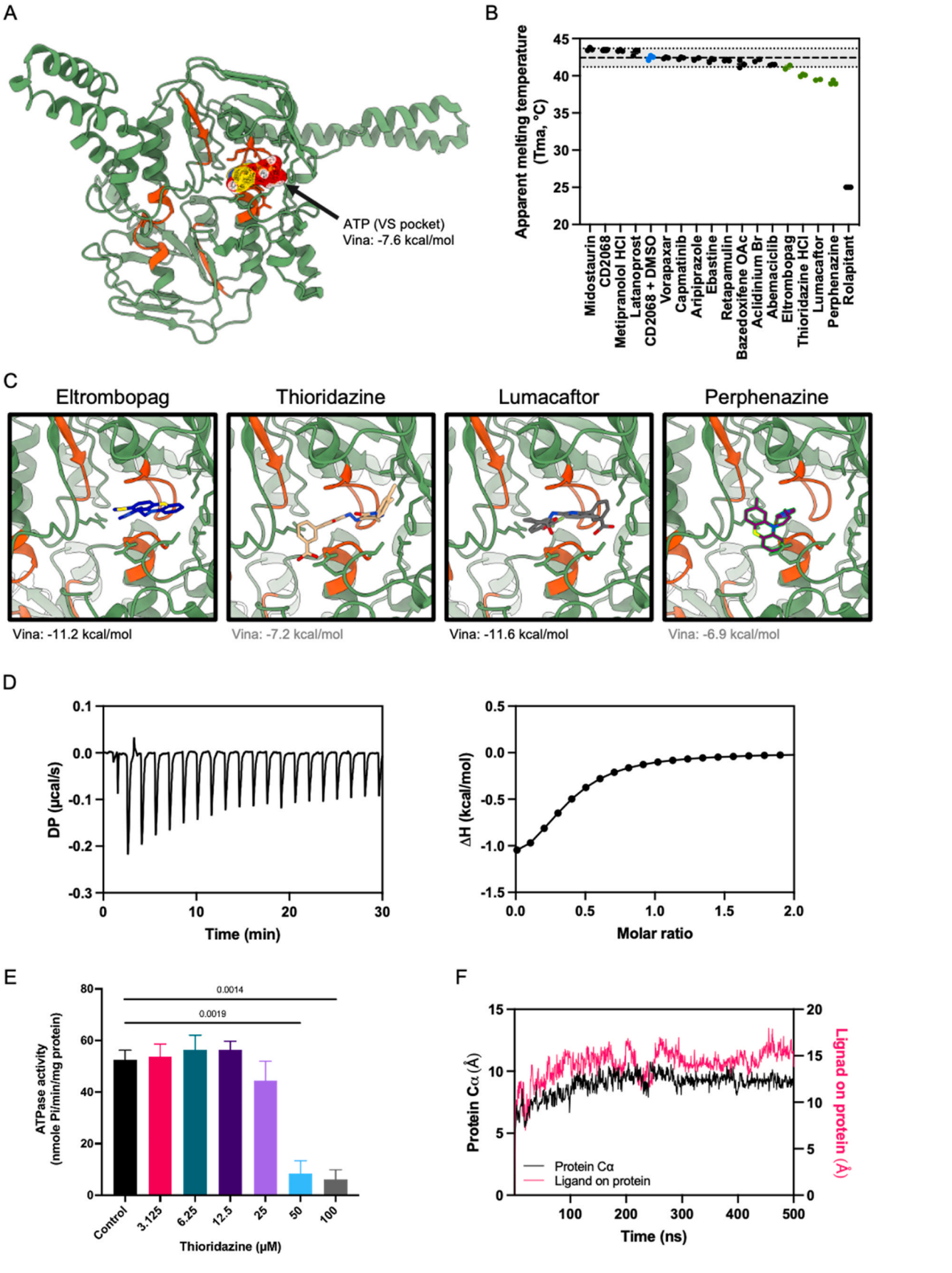

(caption on next page)

Fig. 1. Virtual screening of non-antibiotic FDA-approved drugs targeting CD2068. (A) CD2068 model generated from i-Tasser server used for virtual screening with ATP docked to ATP binding pocket. ATP motifs are colored in orange. (B) Apparent temperature (T_{ma}) of CD2068 with various hits identified from virtual screening by DSF. CD2068 with 0.4 % DMSO as a comparator is shown in blue. Green dots indicate ligands with T_{ma} shift > 5 × SD from Tma_{DMSO} threshold (grey area). Data were from 3 replicates. (C) Docking pose of 4 hits identified from DSF experiment from AutoDock Vina. Hits from FlexX (thioridazine and perphenazine) were redocked using AutoDock Vina (binding energies are shown in grey). (D) Differential power (DP) of each injection needed to maintain the temperature of the sample cell close to the reference cell and integrated heat profile against ligand molar ratio of ITC data. (E) ATPase activity of CD2068 in the presence of various concentrations of thioridazine. Bar represents the mean released inorganic phosphate with the standard error of mean. Statistical significance was determined using an unpaired Student's *t*-test (*p*-value). (F) Protein and ligand on protein RMSD from 500 ns MD simulation of thioridazine on CD2068. (For interpretation of the references to color in this figure legend, the reader is referred to the web version of this article.)

some modifications [23]. Specific-pathogen-free C57BL/6NJcl female mice (6–8 weeks old, ~20 g) were obtained from Nomura Siam International and acclimatized for 8 days with sterile food and water *ad libitum*. After acclimatization, mice were given an antibiotic cocktail to induce dysbiosis, comprising 1.2 mg/mL kanamycin, 0.105 mg/mL gentamycin, 0.645 mg/mL metronidazole, 0.135 mg/mL vancomycin, 2550 U/mL colistin, and 10 mg/mL sucrose for 5 days. After two days of regular water, mice received 10 mg/mL clindamycin intraperitonially. On day 0, mice were challenged with 10^6 spores of *C. difficile* strain R20291 by oral gavage, 2 hours before treatment. For the three treatment groups, mice received a daily dose of either 5 mg/kg thioridazine or 10 mg/kg vancomycin, or 2.5 % DMSO (control) by oral gavage for 5 days. Abnormal behaviors, clinical disease, weight loss, and stool samples were monitored daily. Humane endpoint signs, including > 20 % weight loss, loss of balance, immobilization, and behavioral changes were checked daily. On day 5, all mice were euthanized using CO_2. Mice were handled according to institutional policies for animal health and well-being under approval from the Faculty of Tropical Medicine Institutional Animal Care and Use Committee, Mahidol University (protocol number FTM-ACUC 001/2023). For statistical analysis, a power analysis was performed to determine the minimum sample size needed for each treatment group. The effect size was estimated from prior data or pilot studies, and a significance level (α) of 0.05 and a power of 0.8 were set. Using these parameters, the required sample size per group was calculated to ensure sufficient power to detect meaningful differences between the treatment groups and the control group. For 16 s rRNA gene sequencing, bacterial genomic DNA was extracted from stool using the DNeasy PowerMax Soil kit (Qiagen). The sequencing library was prepared with a Meta VX Library Preparation Kit, targeting the V3 and V4 regions of 16 s rRNA, and sequenced using the Illumina Miseq/Novaseq Platform. OTU clustering was done using VSEARCH clustering (1.9.6) with 97 % similarity against the Silva (v.138) reference database (Vishuo Biomedical). For histopathological analysis, colon tissues were fixed in formalin, embedded in paraffin, sectioned and stained with hematoxylin and eosin. Histopathological damage was scored by an experienced histopathologist in a blinded manner, evaluating inflammatory cell filtration, mucosal architecture, and edema on a four-point scale from 0 (normal) to 3 (severely pathological). The overall severity was the sum of all parameters.

3. Results

3.1. Virtual screening of non-antibiotic FDA-approved drugs targeting CD2068

To generate the CD2068 protein model, seven prediction servers were used: SWISS-MODEL, i-TASSER, trRosetta, Robetta, ModWeb, RoseTTAFold, and AlphaFold. The i-TASSER-2 model, which clustered well with closed ABCF structures from the PDB database, was selected for further analyses (Fig. 1A). To identify novel CD2068 inhibitors via drug repurposing, we performed virtual screening on 1094 non-antibiotic FDA-approved drugs (300–600 Da). AutoDock Vina and SeeSar identified 5 and 15 hits, respectively (Table S1). Top docking results from AutoDock Vina showed binding energies from –10.9 to –11.6 kcal/mol, higher than ATP's –7.6 kcal/mol. These hits included treatments for psychotic disorders, tumors, cardiovascular conditions, impetigo, antiarrhythmics, glaucoma, IBS, vasomotor symptoms, cystic fibrosis, thrombocytopenia, and nausea. Excluding drugs for external use, we further carried out a DSF assay with 17 non-antibiotic hits. Four drugs including lumacaftor, eltrombopag, thioridazine, and perphenazine exhibited ΔT_m values larger than the threshold (Fig. 1B), suggesting their binding interaction with the CD2068 protein (Fig. 1C). These DSF hits were further investigated for binding affinity with CD2068 using ITC. ITC clearly indicated an interaction between thioridazine and CD2068, with a moderate binding constant (K_d) at 14.8 ± 7.6 μM. The initial interaction between thioridazine and CD2068 was exothermic (Fig. 1D), demonstrating a ΔH value of –1.50 ± 0.399 Kcal/mol. These findings confirm the interaction between thioridazine and CD2068.

The inhibitory effect of thioridazine on CD2068 activity was confirmed using an ATP hydrolysis assay. In the presence of 50 μM thioridazine, ATP hydrolysis activity significantly reduced from 52.52 to 8.39 nmole·min^{-1}·mg^{-1} ($p = 0.0019$). At 100 μM thioridazine, ATPase activity further reduced to 6.10 nmole·min^{-1}·mg^{-1} ($p = 0.0014$) (Fig. 1E). The IC_{50} for ATP hydrolysis inhibition was ~30 μM. Furthermore, molecular docking simulation was employed to model interaction of thioridazine with CD2068. Thioridazine was stabilized in CD2068 throughout the simulation run (Fig. 1F).

3.2. Thioridazine inhibits the growth of C. difficile in vitro

For antimicrobial activity, thioridazine inhibited the growth of *C. difficile* ribotype 012 in a concentration-dependent manner, with no growth above 64 μg/mL (Fig. 2A). Thioridazine displayed antimicrobial activity against all tested ribotypes in the range of 64 – 128 μg/mL. Vancomycin's MIC values ranged from 1–4 μg/mL, metronidazole's from 0.25–1 μg/mL, and fidaxomicin's from < 0.00195–0.125 μg/mL (Table 1). Despite requiring higher concentrations compared to other CDI antibiotics, thioridazine exhibited a rapid-killing profile within the first hour, outperforming vancomycin, metronidazole, and fidaxomicin at their corresponding MICs (Fig. 2B). These findings highlight thioridazine's potential as a rapid-acting CDI treatment with broad-spectrum activity against various *C. difficile* ribotypes.

Furthermore, the combination of thioridazine with vancomycin, metronidazole, or fidaxomicin showed an additive effect, with FICIs of 1.0. Specifically, thioridazine at 32 μg/mL combined with sub-MIC concentrations of vancomycin (1 μg/mL, 0.25 × MIC), metronidazole (0.125 μg/mL, 0.25 × MIC), or fidaxomicin (0.0078 μg/mL, 0.125 × MIC) completely inhibited the growth of *C. difficile* ribotype 012, compared to each antibiotic alone (Fig. 2C-E). Taken together, our results indicate the potential of thioridazine to be used as a helper compound to enhance the efficacy of current CDI antibiotics or as an alternative CDI treatment.

3.3. Thioridazine potentially promotes mice survival and restores gut microbial diversity in a CDI mouse model

The inhibition of CD2068 and *in vitro* anti-*C. difficile* activity of thioridazine led to an investigation of its *in vivo* efficacy in a CDI mouse model. Mice were divided into three groups: one receiving 5 mg/kg of thioridazine, another receiving 10 mg/kg of vancomycin, and a control group with no treatment (Fig. 3A). Vancomycin protected 80 % of mice from CDI over five days, while untreated mice did not survive by day 3

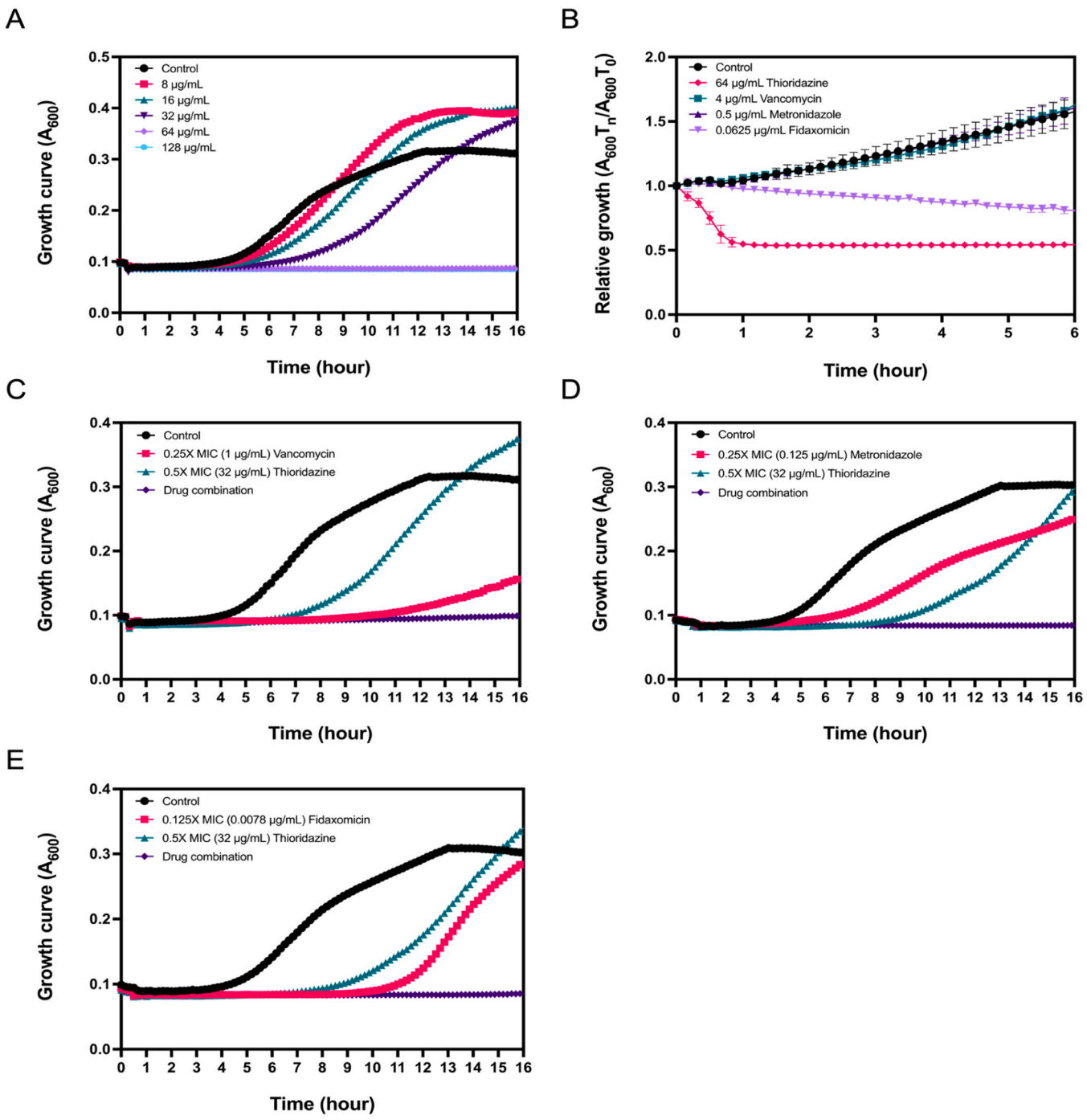

Fig. 2. Thioridazine inhibits the growth of *C. difficile in vitro*. (A) Growth curve of *C. difficile* ribotype 012 under various concentrations of thioridazine. Bacterial growth was monitored by A_{600} every 10 minutes for 16 hours. (B) Initial time-kill kinetics of thioridazine against *C. difficile* ribotype 012. Optical density was measured every 10 minutes for 6 hours. The time-kill curve is represented by the mean relative growth of A_{600} at T_n/T_0 with standard deviation. Effect of combining sub-lethal concentrations of thioridazine and standard CDI drugs on *C. difficile* ribotype 012 growth. Growth was measured by A_{600} every 10 minutes for 16 hours under the challenge with a combination of 32 μg/mL thioridazine and sub-lethal concentrations either of (C) 1 μg/mL vancomycin, (D) 0.125 μg/mL metronidazole, and (E) 0.0078 μg/mL fidaxomicin.

post-challenge. Thioridazine-treated mice exhibited an initial survival rate of 80 % by Day 2, which declined to 20 % by Day 5 (Fig. 3B). Weight loss was observed in both untreated and thioridazine-treated mice on day 2. However, one surviving mouse from the thioridazine-treated group recovered from CDI, regaining weight comparable to the vancomycin-treated group by Day 5 (Fig. 3C). 16S rRNA gene sequencing was used to assess microbial community changes during CDI (Fig. 3D). Significant differences ($p < 0.0001$) in bacterial diversity and richness were noted between the untreated (D-8) and treated groups (D0). The antibiotic cocktail reduced healthy bacteria like *Lactobacillus* and *Muribaculaceae* and increased pathogens such as *Proteus*, *Enterococcus*, and *Parasutterella*. After two days of treatment, microbial structures in thioridazine and vancomycin groups resembled the untreated control. However, the surviving thioridazine-treated group showed microbial diversity similar to healthy controls by day 5, with high levels of beneficial bacteria and minimal *Proteus* compared to vancomycin

Table 1
Antimicrobial activity of thioridazine, vancomycin, metronidazole, and fidaxomicin against *C. difficile* ribotypes.

Ribotype (strain)	MIC (μg/mL)			
	Thioridazine	Vancomycin	Metronidazole	Fidaxomicin
001	64	2	0.25	0.0039
012 (630)	64	2 – 4	0.25 – 0.5	0.03125 – 0.0625
017	64	2	0.5–1	0.03125
020	64	1	0.25 – 0.5	0.0625
023	64	2	0.125	0.0156 – 0.0625
027 (R20291)	64	1 – 2	0.25 – 0.5	0.0625 – 0.125
046	64 – 128	2 – 4	0.25 – 1	0.0156 – 0.03125
056	64	4	0.25	0.0156 – 0.0625
077	64 – 128	4	0.25 – 1	0.0156 – 0.0625
081	64	1 – 2	0.5 – 1	<0.00195
095	64	2 – 4	0.5 – 1	0.0156 –0.0625
106	64	2	0.25 – 0.5	0.0625 – 0.125

group (Fig. 3E).

Histopathological examination (Figs. 3F and 3G) revealed the highest inflammation, epithelial damage, and edema in the untreated group. Inflammatory cell infiltration was consistent across all conditions, a marker of CDI. Thioridazine (5 mg/kg) and vancomycin (10 mg/kg) both significantly reduced epithelial damage compared to the control. The thioridazine group had significant submucosal edema but no difference from the control, while vancomycin effectively reduced edema ($p = 0.0005$). Overall, thioridazine at 5 mg/kg provided suboptimal protection but slightly restored gut community structure similar to healthy controls. Despite moderate efficacy, increasing thioridazine dosage in future studies could enhance its effectiveness in treating CDI.

4. Discussion

Clostridioides difficile remains a concern in public health due to its intrinsic antibiotic resistance, leading to treatment failures and recurrences. Current therapies, including vancomycin, fidaxomicin, and metronidazole, are becoming less effective as resistance increases. Thus, there is an urgent need to develop new treatments. In this study, we employed a computational drug repurposing strategy to identify potential inhibitors targeting CD2068, an ABC protein in *C. difficile*, using FDA-approved non-antibiotic drugs to accelerate the discovery process.

To predict the structure of CD2068, we utilized several protein structure prediction servers that apply homology modeling and/or *ab initio* methods. The models closely resembled the ABCF proteins. We selected the i-TASSER-2 model, featuring a closed conformation, for further analysis due to its alignment with known ABCF structures and functional ATP binding sites. Despite ATP's known interaction with ABCF proteins, docking results showed ATP binding with relatively high energy, suggesting transient interactions. For virtual screening, we used AutoDock Vina and FlexX docking 1094 non-antibiotic FDA-approved drugs into the ATP binding pocket of the CD2068 model. AutoDock Vina identified 5 hits, while FlexX identified 15, but with less precise scoring. We excluded hits like staining dyes and vitamin E and purchased the remaining drugs for further testing. Biophysical methods, including Differential Scanning Fluorimetry (DSF) and Isothermal Titration Calorimetry (ITC), were employed to confirm interactions. DSF showed that four hits—eltrombopag, thioridazine HCl, lumacaftor, and perphenazine—interacted with CD2068, indicated by significant shifts in T_m. However, ITC was limited due to solubility issues and high DMSO concentrations.

Thioridazine emerged as a potential candidate based on our hypothesis that disrupting CD2068 function may increase bacterial susceptibility to antibiotics. Our study provides the first evidence that thioridazine inhibits CD2068 ATPase activity with hydrolysis of ATP being reduced in the presence of 50 μg/mL thioridazine. *In vitro*, thioridazine also lowered the MICs of standard CDI drugs, implying its potential in reversing antimicrobial resistance. This aligns with previous findings of thioridazine's additive and synergistic effects with antibiotics [24,25]. However, the precise mode of action remains unclear. While thioridazine demonstrated antimicrobial activity against *C. difficile*, it is not yet established whether this effect is primarily due to CD2068 inhibition. Previous studies have linked thioridazine to disruptions in cell wall biosynthesis and efflux mechanisms [24], raising the possibility that it affects bacterial permeability and drug uptake. Additional experiments are needed to elucidate its exact mechanism against *C. difficile*.

Thioridazine has demonstrated antibacterial activity against multiple pathogens, including *Staphylococcus aureus*, *Vibrio cholerae*, *Salmonella*, *Shigella*, *Listeria monocytogenes*, *E. coli*, *Bacillus*, *Acinetobacter baumannii*, *Klebsiella pneumoniae*, and *Pseudomonas aeruginosa* [26]. It has also been studied against methicillin-resistant *S. aureus* (MRSA), methicillin-sensitive *S. aureus* (MSSA), *Enterococcus faecalis*, *E. faecium*, and both intracellular and extracellular multidrug-resistant *Mycobacterium tuberculosis*. Reported MICs for thioridazine range from 10 to 32 μg/mL, depending on the bacterial strain [27,28]. In our study, thioridazine inhibited the growth of twelve *C. difficile* ribotypes at 64 – 128 μg/mL, with activity at concentrations similar to those required for ATPase inhibition, suggesting a potential link between these effects.

Given thioridazine's known CNS side effects when used for psychiatric conditions, its feasibility as an anti-infective requires careful evaluation. To assess its potential *in vivo*, we tested thioridazine in a CDI mouse model, administering 5 mg/kg thioridazine and comparing outcome to 10 mg/kg vancomycin and an untreated control group. Vancomycin served as a reference treatment. Based on previous *in vivo* studies, a 10 mg/kg/day thioridazine treatment in a 60 kg pig infected with *S. aureus* for 21 days caused animal behavioral changes, including dizziness and severe agitation. To minimize potential adverse effects and adhere to animal welfare and ethical regulations [29], thioridazine was administered at a lower concentration (5 mg/kg) compared to vancomycin (10 mg/kg), which may have contributed to its less potent therapeutic effect. No observable side effects occurred at this dose during the study period. Thioridazine at 5 mg/kg resulted in 20 % survival compared to 80 % survival with 10 mg/kg of vancomycin. Following our humane endpoint criteria, mice with > 20 % weight loss were euthanized. By Day 3, three mice in thioridazine-treated group met this endpoint, while all untreated control mice succumbed to disease progression. Despite the lower survival rate, the bacterial community in the thioridazine-treated mice demonstrated a partial recovery, resembling that of the healthy control group. By day 5, high bacterial abundance and species richness were noted in the thioridazine group. Healthy gut bacterial indicators, such as *Lactobacillus*, *Muribaculaceae*, and *Lachnospiraceae*, were greatly identified in the thioridazine-treated group, supporting previous studies on probiotic-treated moderate CDI [30]. It has been known that normal gut flora act as a colonization barrier to *C. difficile*, and antibiotics disrupt this balance, facilitating infection. In our study, the community structure was altered after antibiotic cocktail treatment (D0) compared to the healthy control (D-8). Enteric pathogenic bacteria, including *Proteus*, *Enterococcus*, and *Parasutterella* are associated with severe CDI [30]. In particular, *Proteus* has been linked to ulcerative lesions in the gastrointestinal tract of immunodeficient mice [31]. A relative abundance of these bacteria was noted in all conditions after two days of *C. difficile* challenge, and high levels of *Proteus* persisted under vancomycin treatment. Conversely, five-day thioridazine treatment resulted in minimal identification of these pathogenic indicators. This finding may underscore the narrow antimicrobial spectrum of thioridazine compared to current CDI drugs, such as metronidazole and vancomycin, which have broad antibiotic spectra and unacceptably high CDI recurrence rates. Further exploring target and mechanism of action of thioridazine, along with the investigation of mice fecal *C. difficile* bioburden could highlight its antibacterial activity.

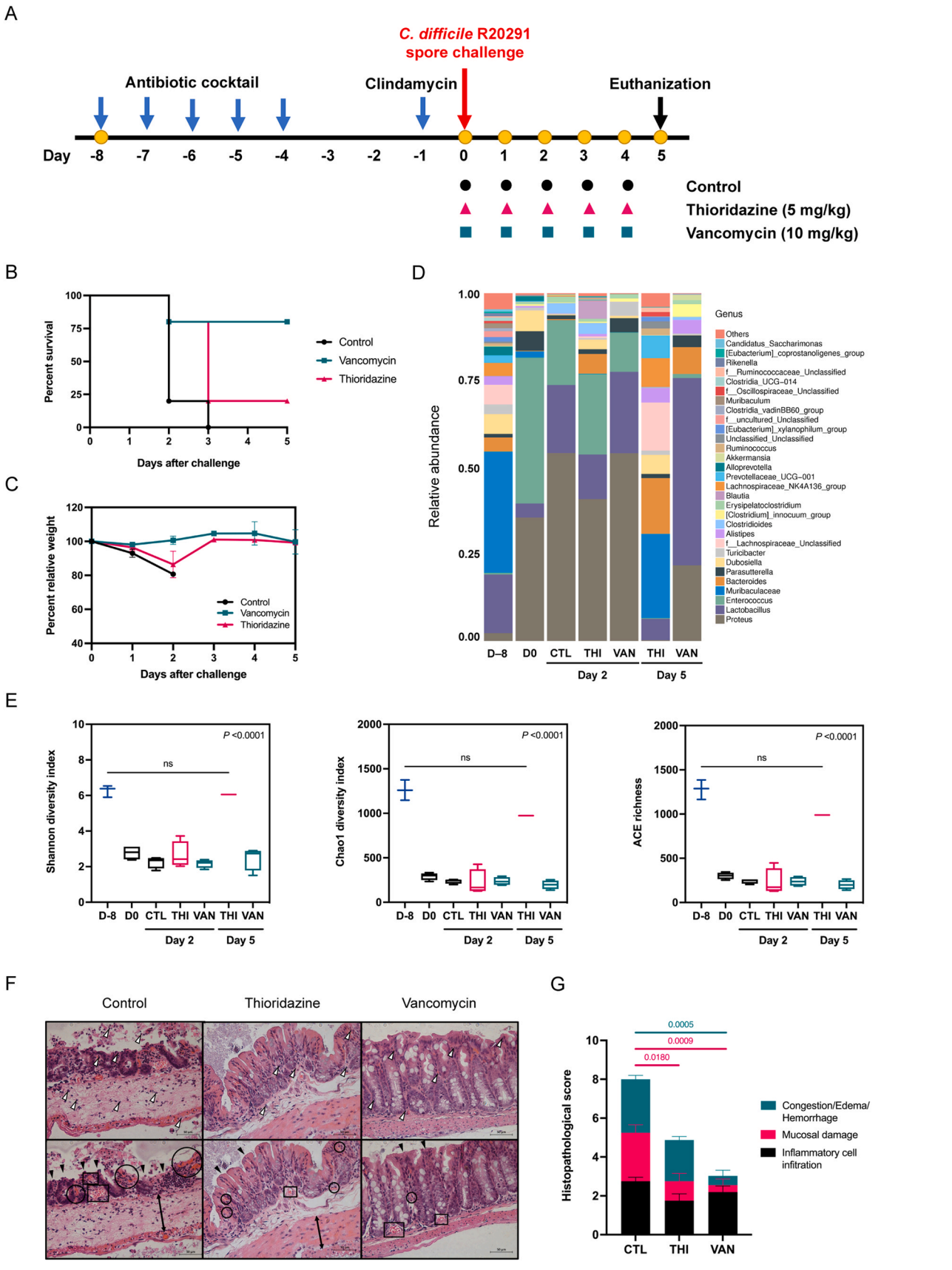

(caption on next page)

Fig. 3. Preclinical validation of thioridazine on anti-*C. difficile* activity in a CDI mouse model. (A) CDI mouse experimental design schematic. Five mice ($n = 5$) were randomly allocated into each treatment group. All mice were pretreated with an antibiotic cocktail for 5 days prior to clindamycin treatment (blue arrow). On day 0, all mice were challenged with *C. difficile* spores (red arrow) and received the first drug treatment two hours post-infection. Mice were treated once daily for 5 consecutive days. Weight and feces were collected once daily (yellow circle) before treatment. At the end of the experiment, all mice were euthanized. (B) Kaplan-Meier survival curve. Mice were treated with thioridazine (5 mg/kg), vancomycin (10 mg/kg) or left untreated for 5 days after *C. difficile* spore challenge. (C) Average relative weight of all surviving mice. Infected mice were treated with thioridazine (5 mg/kg), vancomycin (10 mg/kg), or left untreated for 5 days post-challenge. The weight of all surviving mice was measured daily until the end of the experiment. Data are presented as the percent relative weight (mean ± standard deviation) of each group. (D) Relative abundance of bacterial genus among different groups. Bacterial abundance and diversity of each treatment group were analyzed after drug treatment on days 0, 2, and 5. Non-treated antibiotic cocktail (D-8) was used as a reference control. (E) α-diversity of the microbiome. The microbiome diversity for mice in each treatment group was calculated by Chao1 diversity, Shannon diversity, and Abundance-based coverage estimator (ACE) richness indices. (F) Representative histology of colonic tissues by H&E staining. White arrowheads represent inflammatory cell infiltration, black arrowheads represent mucosal tissue damage, circles represent hemorrhage, squares represent congestion, and double-headed arrows represents submucosa and muscularis edema. (G) Histopathological score of colonic tissue. Histological scores of colonic tissues include epithelial cell damage, neutrophil infiltration, and congestion/edema/hemorrhage. The stack bar represents the mean of each parameter with SEM. At least three microscopic fields were examined. CTL represents the control group, THI represents the thioridazine-treated group, and VAN represents the vancomycin-treated group. (For interpretation of the references to color in this figure legend, the reader is referred to the web version of this article.)

While our study provides preliminary insights into thioridazine's *in vivo* effects, several limitations should be noted. The small sample size, lack of replication, and potential cage effects, which are known confounders in *C. difficile* research, may have influenced outcomes [32]. The lower survival rate in the thioridazine-treated group underscores the need for independent replication with larger cohorts and optimized dosing regimens. Further studies should explore its combination potential with existing CDI treatments and investigate fecal *C. difficile* bioburden to better define its antimicrobial effects. Additionally, medicinal chemistry approaches to develop thioridazine derivatives with reduced CNS side effects while retaining antimicrobial activity could enhance its therapeutic viability.

5. Conclusions

Thioridazine, an antipsychotic drug, demonstrated ATPase inhibition CD2068 and antimicrobial activity against *C. difficile in vitro*. While its *in vivo* effects were less pronounced compared to vancomycin, its potential to modulate gut microbiota and enhance antibiotic efficacy warrants further investigation. Given its known CNS side effects, future studies should explore alternative dosing strategies, combination therapies, and the development of structurally modified derivatives with improved safety profiles. Independent replication with larger animal cohorts will be essential to determine thioridazine's role in CDI treatment.

Author statement

We the undersigned declare that this manuscript is original, has not been published before and is not currently being considered for publication elsewhere. We confirm that the manuscript has been read and approved by all named authors and that there are no other persons who satisfied the criteria for authorship but are not listed. We further confirm that the order of authors listed in the manuscript has been approved by all of us.

We understand that the Corresponding Author is the sole contact for the Editorial process. He is responsible for communicating with the other authors about progress, submissions of revisions and final approval of proofs

Funding

This research project is supported by Mahidol University (Fundamental Fund: fiscal year 2023 by National Science Research and Innovation Fund (NSRF); contract number: FF-058/2566).

CRediT authorship contribution statement

Methinee Pipatthana: Conceptualization, Investigation, Methodology, Visualization, Formal analysis, Writing - Original Draft. **Matthew Phanchana:** Conceptualization, Investigation, Methodology, Visualization, Formal analysis, Writing - Original Draft. **Apiwat Sangphukieo:** Software, Formal analysis. **Sitthivut Charoensutthivarakul:** Investigation, Methodology. **Phurt Harnvoravongchai:** Methodology, Formal analysis. **Surang Chankhamhaengdecha:** Methodology, Formal analysis. **Pattaneeya Prangthip:** Methodology, Investigation. **Pattanai Konpetch:** Investigation. **Chanakarn Sripong:** Formal analysis, Visualization. **Sarawut Wongphayak:** Software. **Tavan Janvilisri:** Conceptualization, Supervision, Project administration, Methodology, Resources, Writing - Review & Editing.

Declaration of Competing Interest

The authors declare that they have no known competing financial interests or personal relationships that could have appeared to influence the work reported in this paper.

Acknowledgements

We thank Peenalin Loyma, Thanyaluk Krasae and Krieangsak Amnuaysookkasem for the laboratory assistance. We thank Mahidol Vivax Research Unit for providing individual ventilated cages for animal experiment. We also acknowledge the Central Equipment Unit, Faculty of Tropical Medicine, for providing the microscope used in this study. The use of Desmond software was under non-commercial license from Desmond Molecular Dynamics System, version 6.9, D. E. Shaw Research New York, NY. We sincerely thank Professor Barney Luttbeg from Oklahoma State University for proofreading the final manuscript.

Appendix A. Supporting information

Supplementary data associated with this article can be found in the online version at doi:10.1016/j.csbj.2025.02.036.

References

[1] Ray MJ, Strnad LC, Tucker KJ, Furuno JP, Lofgren ET, McCracken CM, et al. Influence of antibiotic exposure intensity on the risk of *Clostridioides difficile* infection. Clin Infect Dis 2024. ciae259.
[2] Peng Z, Jin D, Kim HB, Stratton CW, Wu B, Tang Y-W, et al. Update on antimicrobial resistance in *Clostridium difficile*: resistance mechanisms and antimicrobial susceptibility testing. J Clin Microbiol 2017;55:1998–2008.
[3] Harnvoravongchai P, Pipatthana M, Chankhamhaengdecha S, Janvilisri T. Insights into drug resistance mechanisms in *Clostridium difficile*. Essays Biochem 2017;61:81–8.
[4] Pipatthana M, Harnvoravongchai P, Pongchaikul P, Likhitrattanapisal S, Phanchana M, Chankhamhaengdecha S, et al. The repertoire of ABC proteins in *Clostridioides difficile*. Comput Struct Biotechnol J 2021;19:2905–20.
[5] Ngernsombat C, Sreesai S, Harnvoravongchai P, Chankhamhaengdecha S, Janvilisri T. CD2068 potentially mediates multidrug efflux in *Clostridium difficile*. Sci Rep 2017;7:9982.

[6] McDonald LC, Gerding DN, Johnson S, Bakken JS, Carroll KC, Coffin SE, et al. Clinical practice guidelines for *Clostridium difficile* infection in adults and children: 2017 update by the Infectious Diseases Society of America (IDSA) and Society for Healthcare Epidemiology of America (SHEA). Clin Infect Dis 2018;66:e1–48.
[7] Waterhouse A, Bertoni M, Bienert S, Studer G, Tauriello G, Gumienny R, et al. SWISS-MODEL: homology modelling of protein structures and complexes. Nucleic Acids Res 2018;46:W296–303.
[8] Wu S, Skolnick J, Zhang Y. Ab initio modeling of small proteins by iterative TASSER simulations. BMC Biol 2007;5:1–10.
[9] Yang J, Anishchenko I, Park H, Peng Z, Ovchinnikov S, Baker D. Improved protein structure prediction using predicted interresidue orientations. Proc Natl Acad Sci 2020;117:1496–503.
[10] Kim DE, Chivian D, Baker D. Protein structure prediction and analysis using the Robetta server. Nucleic Acids Res 2004;32:W526–31.
[11] Eswar N, John B, Mirkovic N, Fiser A, Ilyin VA, Pieper U, et al. Tools for comparative protein structure modeling and analysis. Nucleic Acids Res 2003;31:3375–80.
[12] Baek M, DiMaio F, Anishchenko I, Dauparas J, Ovchinnikov S, Lee GR, et al. Accurate prediction of protein structures and interactions using a three-track neural network. Science 2021;373:871–6.
[13] Jumper J, Evans R, Pritzel A, Green T, Figurnov M, Ronneberger O, et al. Highly accurate protein structure prediction with AlphaFold. nature 2021;596:583–9.
[14] Dong R, Pan S, Peng Z, Zhang Y, Yang J. mTM-align: a server for fast protein structure database search and multiple protein structure alignment. Nucleic Acids Res 2018;46:W380–6.
[15] Pettersen EF, Goddard TD, Huang CC, Meng EC, Couch GS, Croll TI, et al. UCSF ChimeraX: structure visualization for researchers, educators, and developers. Protein Sci 2021;30:70–82.
[16] Trott O, Olson AJ. AutoDock Vina: improving the speed and accuracy of docking with a new scoring function, efficient optimization, and multithreading. J Comput Chem 2010;31:455–61.
[17] Assempour N, Iynkkaran I, Liu Y, Maciejewski A, Gale N, Wilson A, et al. 5.0: a major update to the DrugBank database for 2018. Nucleic Acids Res 2018;46:D1074–82.
[18] O'Boyle NM, Banck M, James CA, Morley C, Vandermeersch T, Hutchison GR. Open Babel: an open chemical toolbox. J Chemin- 2011;3:1–14.
[19] Bowers KJ, Chow E, Xu H, Dror RO, Eastwood MP, Gregersen BA, et al. Scalable algorithms for molecular dynamics simulations on commodity clusters. In: Proceedings of the 2006 ACM/IEEE Conference on Supercomputing 2006.
[20] Canadell D, Bru S, Clotet J, Ariño J. Extraction and quantification of polyphosphate in the budding yeast Saccharomyces cerevisiae. Bio Protoc 2016;6. e1874-e.
[21] David W. Hecht M.D., and National Committee for Clinical Laboratory Standards. Methods for antimicrobial susceptibility testing of anaerobic bacteria; Approved Standard: NCCLS; 2004.
[22] Balouiri M, Sadiki M, Ibnsouda SK. Methods for in vitro evaluating antimicrobial activity: a review. J Pharm Anal 2016;6:71–9.
[23] Abutaleb NS, Seleem MN. Auranofin, at clinically achievable dose, protects mice and prevents recurrence from *Clostridioides difficile* infection. Sci Rep 2020;10:7701.
[24] Thorsing M, Klitgaard JK, Atilano ML, Skov MN, Kolmos HJ, Filipe SR, et al. Thioridazine induces major changes in global gene expression and cell wall composition in methicillin-resistant *Staphylococcus aureus* USA300. PLoS One 2013;8:e64518.
[25] Kristiansen MM, Leandro C, Ordway D, Martins M, Viveiros M, Pacheco T, et al. Thioridazine reduces resistance of methicillin-resistant *Staphylococcus aureus* by inhibiting a reserpine-sensitive efflux pump. In Vivo 2006;20:361–6.
[26] Christensen JB, Hendricks O, Chaki S, Mukherjee S, Das A, Pal TK, et al. A comparative analysis of in vitro and in vivo efficacies of the enantiomers of thioridazine and its racemate. PLoS One 2013;8:e57493.
[27] Hendricks O, Molnar A, Butterworth TS, Butaye P, Kolmos HJ, Christensen JB, et al. In vitro activity of phenothiazine derivatives in *Enterococcus faecalis* and *Enterococcus faecium*. Basic Clin Pharmacol Toxicol 2005;96:33–6.
[28] Kristiansen MM, Leandro C, Ordway D, Martins M, Viveiros M, Pacheco T, et al. Phenothiazines alter resistance of methicillin-resistant strains of *Staphylococcus aureus* (MRSA) to oxacillin in vitro. Int J Antimicrob Agents 2003;22:250–3.
[29] Stenger M, Behr-Rasmussen C, Klein K, Grønnemose RB, Andersen TE, Klitgaard JK, et al. Systemic thioridazine in combination with dicloxacillin against early aortic graft infections caused by *Staphylococcus aureus* in a porcine model: in vivo results do not reproduce the in vitro synergistic activity. PLoS One 2017;12:e0173362.
[30] De Wolfe T, Kates A, Barko L, Darien B, Safdar N. Modified mouse model of *Clostridioides difficile* infection as a platform for probiotic efficacy studies. Antimicrob Agents Chemother 2019;63. 10.1128/aac. 00111-19.
[31] Zhang J, Hoedt EC, Liu Q, Berendsen E, Teh JJ, Hamilton A, et al. Elucidation of Proteus mirabilis as a key bacterium in Crohn's disease inflammation. Gastroenterology 2021;160:317–30. e11.
[32] Tomkovich S, Stough JM, Bishop L, Schloss PD. The initial gut microbiota and response to antibiotic perturbation influence *Clostridioides difficile* clearance in mice. Msphere 2020;5. https://doi.org/10.1128/msphere. 00869-20.